Bioactive Materials 5 (2020) 859–870

Contents lists available at ScienceDirect

Bioactive Materials

journal homepage: http://www.keaipublishing.com/biomat

Alendronate loaded graphene oxide functionalized collagen sponge for the dual effects of osteogenesis and anti-osteoclastogenesis in osteoporotic rats

Yuyang Zeng[a,b,1], Muran Zhou[a,b,1], Lifeng Chen[a,b], Huimin Fang[a,b], Shaokai Liu[a,b], Chuchao Zhou[a,b], Jiaming Sun[a,b,**], Zhenxing Wang[a,b,*]

[a] Department of Plastic Surgery, Union Hospital, Tongji Medical College, Huazhong University of Science and Technology, Wuhan, 430022, China
[b] Wuhan Clinical Research Center for Superficial Organ Reconstruction, Wuhan, 430022, China

ARTICLE INFO

Keywords:
Osteoporosis
Osteoporotic bone defect
Graphene oxide
Osteoclast
Alendronate

ABSTRACT

Graphene Oxide (GO)-related hydrogels have been extensively studied in hard tissue repair, because GO can not only enhance the mechanical properties of polymers but also promote osteogenic differentiation of mesenchymal stem cells. However, simple GO-related hydrogels are not ideal for the repair of osteoporotic bone defects as the overactive osteoclasts in osteoporosis. Alendronate (Aln) is known to inhibit osteoclasts and may bind to GO through covalent connection. Therefore, delivering Aln in GO-related hydrogels may be effective to repair osteoporotic bone defects. Here, we developed a control-released system which is constructed by collagen (Col)-GO sponges loaded with Aln (Col-GO-Aln) for osteoporotic bone defect repair. *In vitro*, Col-GO-Aln sponges prolonged the release period of Aln, and the sponge containing 0.05% (w/v) GO released Aln faster than sponge with 0.2% GO. Furthermore, tartrate-resistant acid phosphatase (TRAP) and F-actin staining demonstrated that Col-GO-Aln sponges effectively inhibited osteoclastogenesis of monocyte-macrophages. *In vivo*, micro-CT scan showed that the volume of newborn bone in defect site by 0.05% GO sponge was nearly three times larger than that of other groups. Moreover, the CT and histological examinations of rat femur proved that Col-GO-Aln sponges decreased the number of osteoclasts and suppressed the systemic bone loss in osteoporotic rats. These findings reveal that the application of GO as carriers of anti-osteoporosis drugs is a viable treatment for osteoporosis. The results also underscore the potential of GO-related hydrogels with Aln-releasing capacity for bone regeneration in osteoporosis.

1. Introduction

Graphene oxide (GO), a derivative of carbon nanomaterial, has ignited increasing research interests in various fields from electronics to biotechnology [1]. Its structure comprises carbon atoms that condense into a two-dimension honeycomb lattice with multiple oxygen groups, such as carboxyl, hydroxyl, or epoxy, decorated on the basal planes and edges. This special structure enables molecule to exhibit a large specific surface area, high Young's modulus, good thermal conductivity and rich functionalization sites [2]. So that, these good physicochemical and biological properties make GO potentially useful in drug/gene delivery, biosensing, cancer therapy, tissue engineering and other biomedical fields [3–5].

GO related hydrogels have attracted attention in recent years, because incorporation of GO modifies the surface topology of hydrogels and adds various functionalities to hydrogel simultaneously [6]. Natural polymers, such as collagen, chitosan and hyaluronic acid have been widely studied as scaffolds in application of tissue regeneration. This is due to their inherent hydrophilicity, biocompatibility and biodegradability [7]. However, poor mechanical strength of these hydrogels limit their application in hard tissues regeneration, like bone [8]. Studies have demonstrated that addition of GO to these hydrogels helps improve their mechanical properties through establishment of chemical bonds with natural polymers. For instance, Wang's group reported that

Peer review under responsibility of KeAi Communications Co., Ltd.
* Corresponding author. Department of Plastic Surgery, Union Hospital, Tongji Medical College, Huazhong University of Science and Technology, Wuhan, 430022, China.
** Corresponding author. Department of Plastic Surgery, Union Hospital, Tongji Medical College, Huazhong University of Science and Technology, Wuhan, 430022, China.
E-mail addresses: sunjm1592@sina.com (J. Sun), benjamin.wzx@163.com (Z. Wang).
[1] These authors contributed equally to this work.

https://doi.org/10.1016/j.bioactmat.2020.06.010
Received 25 April 2020; Received in revised form 7 June 2020; Accepted 14 June 2020

a GO-functionalized collagen scaffold had enhanced mechanical strength and resulted in a remarkable effect when used to repair bone defects [9]. Similarly, Fan and colleagues manufactured a chitosan scaffold bonded with GO that possessed 3-times more mechanical strength and resulted in good bone regeneration effects when implanted into the calvarial bone defect in rats [8]. At the same time, GO has been found to enhance mesenchymal stem cells (MSCs) osteogenic differentiation through concentrating growth factors via π–π bonding [10,11]. These reports demonstrated the prospect of GO to functionalize hydrogels for bone regeneration, but they did not investigate the effect of GO-related hydrogels on repair of bone defect under bone metabolic disorders. Proliferation and osteogenic differential ability of MSCs were impaired under bone metabolic disorders [12,13]. Furthermore, the disordered microenvironment, such as growth factor deficiency, hypoxia and inflammatory response, is not conducive to bone regeneration [14,15]. These make it difficult for GO-related hydrogels to repair bone defects under bone metabolic disorders.

Osteoporosis is a common bone metabolic disorder disease, characterized by excessive activation of the osteoclast and functional decline of the osteoblast [16]. Bone loss eventually occurs when there is disrupted balance between bone resorption and formation. Patients who suffer from this condition are likely to encounter bone fractures and have an increased risk of delayed and/or non-union [17]. Several viewpoints regarding repair of bone defects in osteoporosis have been proposed. For instance, autologous and allogeneic bone grafts are often considered in clinical practice, but they are generally limited by inherent disadvantages including donor site morbidity and high costs [18]. Meanwhile, the disordered microenvironment of bone metabolism further compromises success of bone regeneration via bone tissue graft [15]. To address the problem of bone disorder, administration of drugs such as bisphosphonates, parathyroid hormone and strontium has been used to rebalance the general microenvironment from overactive bone resorption towards harmonious bone metabolism. However, drug concentration is often insufficient due to a lack of blood circulation at the defect site [19,20]. Other studies have reported injection of autologous MSCs into the defect site to promote bone regeneration [21]. Unfortunately, unsatisfactory effects have been achieved owing to reduced ability of osteogenic differentiation in stem cells isolated from patients with osteoporosis [13,21]. In recent years, biomaterials are used to repair osteoporotic bone defects due to its availability of rich sources, low prices and no additional damage [22]. Furthermore, administration of these materials at the defect site provides an appropriate surface for cell ingrowth and attachment, which facilitates bone regeneration [23,24]. Nevertheless, the disordered bone microenvironment still exists and affects the formation of bone tissue. Biomaterials that can effectively deliver drugs, cytokines and genes in situ to facilitate recovery of bone metabolism are preferred for applications in repairing osteoporotic bone defect [25,26].

Alendronate (Aln), a bisphosphonate containing a primary amino group, is a first-line drug in clinical treatment of osteoporosis. Studies have shown that Aln promotes osteogenic differentiation of MSCs and inhibits osteoclastogenesis of monocyte-macrophage [27,28]. Functionally, this drug acts to rebalance bone metabolism of osteoporosis. However, the efficacy of oral administration of Aln to treat osteoporosis is limited by its low bioavailability (0.9–1.8%), instability in digestive juices, and side effects including severe gastrointestinal reactions and bisphosphonate-related osteonecrosis of the jaws [29]. Binding Aln to biomaterials provides an alternative approach for the repair of bone defects in osteoporosis, because it facilitates bypassing absorption in the digestive tract and increases concentration of drugs at the defect site. Previous study has demonstrated that the primary amino group of Aln can link to GO via forming amide bond with the help of 1-(3-dimethylaminopropyl)-3-ethylcarbodiimide hydrochloride (EDC) [30]. We hypothesized that GO-related hydrogels could facilitate the efficient release of Aln at defect sites and enable repair of osteoporotic bone defects.

In this study, we combined GO, Aln and Type I collagen (Col), a common natural polymer, to fabricate Col-GO-Aln sponge and investigated its ability to repair bone defect in osteoporosis. Systematic experiments were conducted to evaluate the physiochemical characterization, drug release property and biocompatibility of the fabricated sponge. Moreover, we studied effects of the Col-GO-Aln sponge on osteogenic differentiation of MSCs isolated from rat bone marrow (BMSCs) and osteoclastogenesis of macrophages derived from rat bone marrow (BMMs) *in vitro*, and evaluated the ability of the sponge to repair bone defects as well as attenuate bone loss in osteoporotic rats.

2. Methods

2.1. Materials and animals

Type I collagen was purchased from Kele Biotech (China), graphene oxide was obtained from Suzhou Tanfeng Tech (China). Aln, EDC and N-hydroxysuccinimide (NHS) were purchased from Sigma-Aldrich (USA). Dulbecco's modified Eagle's medium (DEME) and α-minimal essential medium (α-MEM) were purchased from Hyclone (USA). Fetal bovine serum (FBS), penicillin-streptomycin (PS) and other reagents about cell culture were obtained from Gibco (USA). Recombinant Macrophage Colony stimulating Factor (M-CSF) and Receptor Activator of Nuclear Factor-κ B Ligand (RANKL) were purchased from R&D Systems (USA). Other reagents, unless mentioned specifically, were purchased from Sinopharm Chemical Reagent (China).

All animals used in this study were purchased from the animal center of Huazhong University of Science and Technology (HUST) and the experimental protocols concerning animal were approved by the Animal Ethical Committee of HUST.

2.2. Fabrication of col-GO-Aln Sponges

The Col-GO-Aln sponges were fabricated by chemical cross-linking as our previous report [31]. Briefly, 1 mL Col solution (2% w/v in 0.05 M acetic acid) was homogeneously mixed with GO solution (8 mg/mL) under ultrasound, at a series of different volume ratios to produce different final concentrations of GO (0, 0.05, 0.1, 0.2, 0.3 and 0.5% w/v) in hydrogel. A solution containing 5 mg Aln was subsequently added to the mixture and the final volume topped up to 2 mL. Then, 40 μL of the hydrogel were cast in molds (5 mm in diameter and 2 mm in height) to obtain a porous sponge through freeze-drying, and chemically cross-linked by immersing the contents in a 95% ethanol solution containing 50 mM EDC and 12.5 mM NHS. After 6 h of incubation, the sponges were rinsed five times using double distilled water (ddH_2O) and re-lyophilized, the rinsed ddH_2O was collected for further determining about eluted Aln. Unloaded sponges were fabricated using the same procedure but without adding Aln.

2.3. Characterization of fabricated sponges

The surface and pore morphologies of Col-GO-Aln sponges were characterized by a scanning electron microscopy (SEM; Nova NanoSEM 450, FEI, USA). Porosity of the sponges was determined using the ethanol displacement method reported previously [24]. Briefly, the radius (R), thickness (H) and dry weight (W_1) of each sponge were measured. Then, the sponges were immersed in ethanol for 24 h, and the wet weight (W_2) was measured. The porosity of Col-GO-Aln sponge was calculated as,

$$\text{Porosity} = (W_2 - W_1) / (\rho \times \pi \times R^2) \times H \times 100\%$$ (ρ is the density of ethanol)

The water uptake and retention rates of sponges were evaluated according to previous literature [31]. After immersed in ddH_2O at room temperature for 24 h, the sponges were wiped with a filter paper and

weighed (W_3). Subsequently, the sponges were centrifuged at 500 rpm for 3 min and weighted again (W_4). The water uptake and retention rates were calculated as,

$$\text{Water uptake rate} = [(W_3 - W_1) / W_1] \times 100\%$$

$$\text{Water retention rate} = [(W_4 - W_1) / W_1] \times 100\%$$

Functional groups of sponges were analyzed via Fourier Transform Infrared spectroscopy (FT-IR; VERTEX 70, Bruker, Germany) from 4000 to 500 cm^{-1} with a resolution of 2 cm^{-1}. The chemical compositions were confirmed by Dispersive Raman microscope (FRA 106/s, Bruker, Germany) with a laser at 532 nm. The crystalline phases of sponges were identified using an X-ray diffractometer (XRD; Empyrean, PANalytical B.V., Belgium) in a 2θ range from 5° to 40°.

2.4. Drug release property of col-GO-Aln sponges

The Col-GO-Aln sponges were immersed in 2 mL ddH_2O at 37 °C with shaking at 60 rpm. At predetermined time points (0.5, 1, 1.5, 2, 4, 6, 8, 12, 16, 20, 24 and 30 days), the supernatant was collected and 2 mL ddH_2O was added in return. The concentration of released Aln in supernatant was assayed using spectrophotometric as described in the previous literature [32]. Additionally, the concentration of eluted Aln in the rinsed ddH_2O collected in the fabricated process was also determined to calculate the loading capacity of Col-GO-Aln sponges.

2.5. Isolation and culture of BMSCs

BMSCs were isolated using the method described in previous report [24]. Briefly, two 7-day-old Sprague-Dawley (SD) rats were sacrificed and the femurs were collected aseptically. BMSCs were flushed out from the bone marrow with DMEM containing 1% PS. After collected and washed, the obtained cells were cultured in DMEM supplemented with 10% FBS and 1% PS. BMSCs in Passage 3–4 were used in the following test.

2.6. Adhesion and viability of BMSCs in fabricated sponges

The adhesion and viability of BMSCs in fabricated sponges were evaluated according to the previous literature [8]. Briefly, the sponges were placed in 12-well plates in advance. BMSCs were seeded on sponge at 2×10^4 per 50 μL media and then kept in a cell incubator for 2 h. Subsequently, 1 mL media was added into the well and changed every other day. To evaluate the adhesion and viability of BMSCs in fabricated sponges, the cell-sponge constructs were stained using a Live/Dead assay after 7 days of culture. Observing by a laser scanning confocal microscopy (A1Si, Nikon, Japan), living cells were stained with fluorescein diacetate (FDA, Sigma) and dead cells were stained with propidium iodide (PI, Sigma). To further evaluate the morphology of adherent cell at day 7, the cell-sponge constructs were fixed in 2.5% glutaraldehyde for 30 min and washed with PBS to remove residual fixatives. Subsequently, the constructs were dehydrated through a graded tertiary butanol series and sputter-coated with platinum for SEM analysis.

2.7. Effects of fabricated sponges on proliferation of BMSCs

The extracts of fabricated sponges were prepared as previously reported [33]. Briefly, sponges with or without Aln were immersed in 0.5 mL DMEM and placed in an incubator with 5% CO_2 at 37 °C. The extracts were collected and new DMEM was added in return every 3 days. After 14 days, the cumulative extracts were supplemented with 10% FBS and 1% PS for the following study.

BMSCs were seeded in 96-well plate at 2×10^3 per well and cultured with extracts of different fabricated sponges. After culturing for 1, 3 and 7 days, the attached cells were quantitatively assessed using a Cell Counting Kit-8 (CCK-8, Dojindo, Japan) to investigate the effects of sponges on cell proliferation.

2.8. Effect of fabricated sponges on osteogenic differentiation of BMSCs in vitro

2.8.1. Alkaline phosphatase (ALP) staining and ALP activity assay

BMSCs were seeded in 24-well plate at a density of 2×10^4 cell per well, and cultured with the extracts of fabricated sponges. After culturing for 7 days, the cells were fixed in 4% paraformaldehyde and stained using an ALP Color Development Kit (Beyotime). Moreover, a quantitative analysis about the ALP activity of BMSCs treated with extracts for 7 days was performed according to the manufacturer's instruction of ALP Assay Kit (Beyotime).

2.8.2. Alizarin red staining (ARS) and semiquantitative analysis

BMSCs were seeded in 24-well plate and cultured with DMEM containing 10% FBS and 1% PS. After the adherent cells reached 70–80% confluence, the medium was replaced with extracts of fabricated sponges supplemented with 1 mM dexamethasone (Sigma), 10 mM ascorbate (Sigma) and 1 M β-glycerophosphate (Sigma). After another culturing for 15 days, BMSCs were fixed in 4% paraformaldehyde and incubated with ARS staining solution (Cyagen, China). A semiquantitative analysis of the absorbance at 562 nm was performed to investigate the osteogenic differentiation ability of BMSCs.

2.9. Isolation and culture of BMMs

Primary bone monocyte-macrophages were isolated from female SD rats weighing about 100 g as previously reported [34]. Briefly, the femurs and tibias were separated aseptically, then the marrow cells were washed out using α-MEM. After removing red blood cells, the residual marrow cells were cultured in α-MEM complete medium (α-MEM containing 10% FBS and 1% PS). Subsequently, suspended cells were collected after incubating for 16 h to remove BMSCs and cultured in α-MEM complete medium supplemented with 30 ng/mL M-CSF. The cell morphology of BMMs were observed using a microscope (CKX41, Olympus, Japan) after culturing for 48 and 72 h.

2.10. Effect of fabricated sponges on osteoclastogenesis of BMMs in vitro

2.10.1. Effects on viability of BMMs

BMMs were seeded in 96-well plate at a density of 8×10^3 cells per well and cultured with α-MEM complete medium containing 30 ng/mL M-CSF for 12 h. The extracts of fabricated sponges were prepared using α-MEM according to the above protocol. Subsequently, the cells were treated with extracts supplemented with 30 ng/mL M-CSF and the media were changed every two days. After culturing for 4 days, a CCK-8 assay was performed to evaluate the effects of sponges on viability of BMMs.

2.10.2. Effects on osteoclastogenesis of BMMs

BMMs were seeded in 96-well plate at 8×10^3 cells per well and cultured with extracts supplemented with 30 ng/mL M-CSF and 50 ng/mL RANKL, and the media were changed every two days. Four days later, the cells were fixed in 4% paraformaldehyde for 30 min at 4 °C and stained with a Tartrate-resistant Acid Phosphatase (TRAP) Staining Kit according to the manufacturer's instruction (Sigma). Subsequently, to investigate the effects on osteoclastogenesis, the number and area of TRAP (+) cells were quantified from 5 TRAP staining pictures of BMMs treated with extracts of different sponges using Image-Pro Plus software (Media Cybernetics, USA).

To further observe the influences of fabricated sponges on osteoclastogenesis of BMMs, the immunofluorescence staining of F-actin rings were performed as previously reported [34]. Briefly, BMMs were cultured with extracts containing M-CSF and RANKL for 4 days as above

described. After fixed with 4% paraformaldehyde and washed twice with PBS, the cells were stained with Phalloidin and DAPI according to the manufacturer's protocol (AAT bioquest, USA). The immunofluorescence images were captured via the laser scanning confocal microscope and analyzed using Image-Pro Plus software to evaluate the number and area of the formed F-actin rings.

2.11. In vivo studies

2.11.1. Preparation of osteoporotic rat model

The osteoporotic rat model was prepared via bilateral ovariectomy as previously described [35]. Briefly, SD rats weighing about 200 g were anesthetized with injection of pentobarbital sodium (30 mg/kg, Sigma) by intraperitoneal injection. Subsequently, 2 cm-length skin incisions were made in the lower abdomen to expose the ovary of rat. Then, some rats underwent bilateral ovariectomy (OVX) and some rats, which were cut off an equal volume of parovarian fat, acted as control (Sham). After 3 months, the rats were sacrificed under overdose injection of pentobarbital sodium, and the femurs of rat were collected and subjected to micro-CT (Skyscan 1176, Bruker, Germany) and histological analysis. For micro-CT analysis, an upper 2.2 mm region beginning at 1.0 mm proximal to the medial condyle of femur was set as the region of interest (ROI). Analysis of micro-CT data using CT Analyzer software (Bruker) and H&E staining of distal femoral metaphysis were accomplished to evaluate the degree of bone loss in ovariectomized rat.

2.11.2. Implantation of fabricated sponges in calvarial defects of OVX rats

After ovariectomy 3 months, the rats were anesthetized by pentobarbital (30 mg/kg) intraperitoneal injection and a sagittal incision measuring 1.5 cm in length was made on scalp to access the skull of rat. Subsequently, a full-thickness defect was drilled on the skull using a 5 mm diameter trephine and the fabricated sponges were implanted into the defects. Then the skin incisions were closed and disinfected. The OVX rats (n = 24) were divided into four groups according to the implanted sponges: (1) Col-0.05%GO; (2) Col-0.05%GO-Aln; (3) Col-0.2%GO; (4) Col-0.2%GO-Aln. Three months later, the animals were euthanized with overdose injection of pentobarbital sodium, and the skulls and left femurs were separated and fixed in 4% paraformaldehyde for the following micro-CT and histological evaluation. At the same time, livers, kidneys and cerebrums of rats were collected to determine the toxicity of fabricated sponges using H&E staining.

2.11.3. Evaluation of osteoporotic calvarial defects repair

The collected skulls (n = 6) in each group were assessed with a micro-CT scanner and the morphology of regenerated bone tissue in calvarial defect was reconstructed using VGstudio software (Volume Graphics, Germany). CT Analyzer software was used to calculate the new bone volume (BV) and the percentage of new bone volume relative to tissue volume (BV/TV).

Histological analysis was performed to further evaluate the repair of bone defects. The skull samples were decalcified by daily change of 10% EDTA for 2 weeks, and then they were dehydrated via a graded alcohol series and embedded in paraffin. After cutting the samples into sections in 5 μm thickness, H&E and Masson's Trichrome (Masson) staining were performed respectively to visualized the bone tissue in defect site. Moreover, a osteocalcin (OCN) immunohistochemical staining was performed according to the manufacturer's protocol (Proteintceh Group, China). The images of histological analysis were captured by a Nikon Ni microscope.

2.11.4. Evaluation of attenuating bone loss in OVX rat

The separated femurs (n = 6) were scanned by micro-CT to evaluate the suppression on bone loss, and an upper 2.2 mm region of bone trabecula beginning to distal femur metaphysis was set as ROI. 3D reconstruction images of bone trabecula on lateral and coronal views were visualized using CTvox software (Bruker), and the parameters like BV/TV, bone mineral density (BMD), number of trabecular bone tissue (Tb.N) and separation of trabecular bone tissue (Tb.S) were quantified using CT Analyzer software.

H&E and Masson staining were performed to evaluate the number of trabecular bone in distal femur metaphysis. Additionally, the TRAP staining was used to specially color the osteoclasts on the surface of bone trabecula, and representative indexes of bone resorption, like osteoclast surface relative to trabecular bone surface (OC.S/BS) and number of osteoclast per trabecular bone surface (N.OC/BS), were quantified via measuring 5 sections of each femoral metaphysis as previously reported [36].

2.12. Statistical analysis

All data collected in this work were expressed as mean ± SD and analyzed with SPSS 21.0 software (IBM, USA). A Student's *t*-test was used for the comparisons between two groups and one-way analysis of variance test with post hoc contrasts by Newman-Keuls test was used to analyze differences in multiple comparisons. $P < 0.05$ was considered to be a statistically significant difference.

3. Results

3.1. Fabrication of the col-GO-Aln sponges

Crosslinking and lyophilization procedures resulted in successful generation of a series of drug-loaded sponges containing proportions of GO that ranged from 0 to 0.5% w/v (Fig. S1). The hydrogel without GO (Col-Aln sponge) was white in color, while GO-based ones appeared brown. In addition, an increase in GO proportion gradually darkened the sponges. Fig. 1A illustrated the formation of amide bond between the carboxyl groups of GO and the amino groups of Col or Aln. We observed that the Col-0.3%GO-Aln sponge exhibited a loose interconnection in structure, and the Col-0.5%GO-Aln was shapeless and disruptive (Fig. S1). After the fabricating process, a drug-loaded sponge with GO proportion of 0–0.2% formed stable and porous structures. Therefore, to evaluate the effects of GO on hydrogels for sustained drug delivery and bone regeneration, we selected the 0.05% and 0.2% as the representative concentration for further investigation.

3.2. Characterization of the fabricated sponges

Digital photographs revealed the color and size of our fabricated sponges containing 0.05% and 0.2% GO. Furthermore, we noted that addition of Aln resulted in no significant effect on appearance of the sponges (Fig. 1B). Analysis of SEM images indicated that sponges exhibited a highly porous and network-like internal structure (Fig. 1C).

Physicochemical characterizations such as porosity, water uptake and retention ability are considered important parameters of biomaterials in absorption of tissue fluids and nutrient transport [6]. In this study, the Col-0.05%GO, Col-0.05%GO-Aln, Col-0.2%GO and Col-0.2%GO-Aln sponges respectively exhibited a porosity of 83.47 ± 6.71%, 88.73 ± 6.73%, 84.53 ± 4.15% and 84.78 ± 2.91%, with no statistical significances (Fig. 2A). Nevertheless, comparisons within Col-0.05%GO sponge (5756% uptake and 1915% retention rates) and Col-0.2%GO sponge (5259% uptake and 1802% retention rates) showed a decrease in water uptake and retention ability. This trend was also observed when Col-0.05%GO-Aln was compared to Col-0.2%GO-Aln sponges (Fig. 2B). Besides, Aln had no influence on water uptake and retention appearance of the sponges.

The porosity of the sponges was not altered by the addition of Aln and GO (A) but the water uptake and retention rate of the sponges were reduced following addition of 0.2% GO into the system (B). (n = 5, n.s: no significance, *: $P < 0.05$) (C) The cumulative release curve showed the sustained release of Aln for at least 30 days. Moreover, the Col-

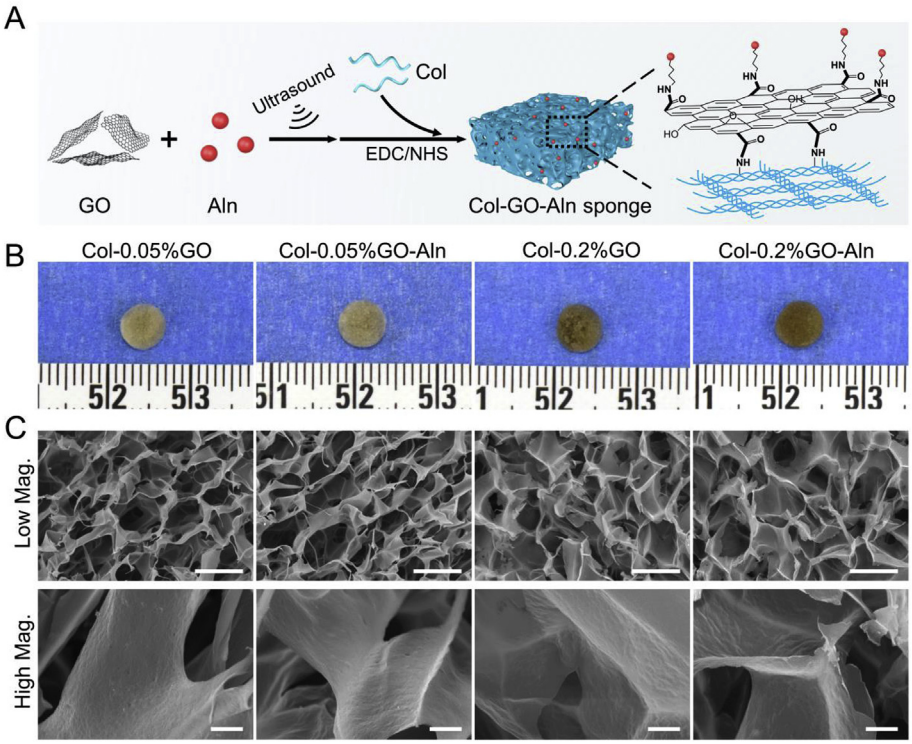

Fig. 1. Schematic illustration of the fabrication procedure and morphology of Col-GO-Aln sponges. (A) Illustration of the fabrication procedure of the Col-GO-Aln sponges and the molecule linking in sponges. Macroscopic images (B) showed that the color of the sponges become progressively darker as the proportion of GO increased. Microscopic images (C) exhibited the highly porous and interconnected structure of sponges. (scale bars in B: 1 cm; in C: 100 μm (Low Mag.) and 10 μm (High Mag.)).

0.2%GO-Aln sponge showed a slower release rate of Aln compared to Col-0.05%GO-Aln sponges. (D) The typical peaks of amide bonds (gray band) and hydroxyl groups of Aln (arrowheads) characterized by FTIR indicated that the Aln was successfully crosslinked in the Col-0.05%GO-Aln and Col-0.2%GO-Aln sponges. (E) In the Raman spectrum, D bond and G bond, the typical bonds in GO were found in all of the four sponges. (F) XRD spectra indicated that the crystalline structures of GO and Aln were disappeared and the fabricated sponges exhibited amorphous crystalline structures.

Properties of Col-0.05%GO-Aln and Col-0.2%GO-Aln sponges to release Aln were investigated *in vitro*. The calculated drug-loading rate of Col-0.05%GO-Aln sponge was 45.40 ± 3.12% and the Col-0.2%GO-Aln sponge was 48.12 ± 1.99%, and there existed no significance. Cumulative release curve showed that Aln could be sustainably delivered for at least one month and the total amount released was about 30 μg (Fig. 2C). The first period involved fast release of Aln at average rate of 4.5 μg/d for 4 days with GO exhibiting no obvious influence on this process. In the following period, the release rate slowed down and was sustained towards the end of the study. Particularly, Aln release from Col-0.05%GO-Aln sponge was faster than that of Col-0.2%GO-Aln.

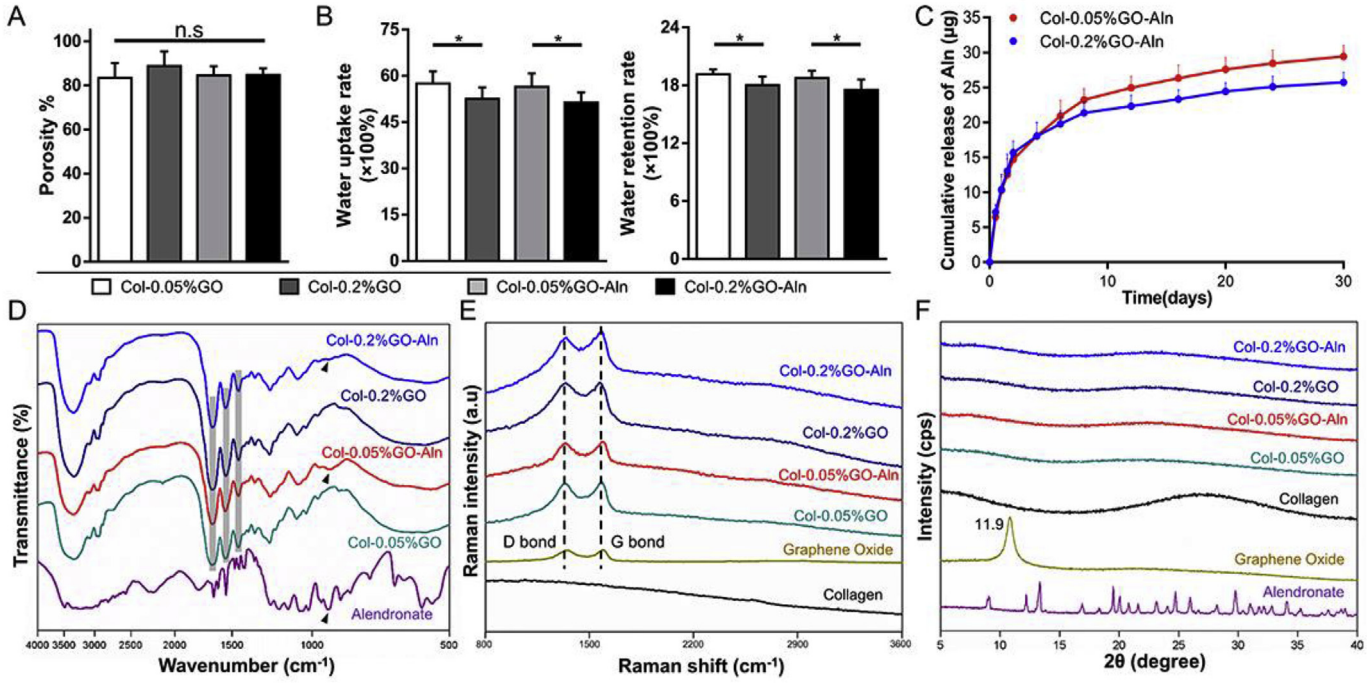

Fig. 2. Physicochemical characteristics and drug release dynamics of the Col-GO-Aln sponges.

We then used the FT-IR spectrum to confirm the chemical structures of the sponges and these results are shown in Fig. 2D. After the crosslinking reactions, the peak of carboxyl groups in GO (1730 cm^{-1}) was significantly diminished; stretching vibrations of amide I (C═O, around 1640-1660 cm^{-1}), and bending vibrations of amide II and amide III (-N-H, around 1544–1554 and 1448-1456 cm^{-1}) were observed in all four sponges (gray band) indicating formation of amide bonds (–NHCO–) [37]. The transmittance of amide I, II, III in Col-0.2%GO and Col-0.2%GO-Aln sponges was higher than that in Col-0.05%GO and Col-0.05%GO-Aln sponges, which indicated that an increase in GO had caused more amide bond formation between carboxyl of GO and amino of Col or Aln [30,37]. A characteristic peak at 926 cm^{-1} for hydroxyl group of Aln appeared in the Col-0.05%GO-Aln and Col-0.2%GO-Aln sponges, implying presence of the drug [38]. Due to the relatively low concentration (0.05% and 0.2%) of GO incorporated in drug-loaded sponge, the FT-IR spectrum was not sensitive to the existence of GO. To identify the GO in Col-GO-Aln sponges, we measured the Raman spectrum, a highly sensitive method for detection of conjugated and double carbon–carbon bonds. The results revealed two peaks of 1355 and 1593 cm^{-1} (D and G bands) in all sponges (Fig. 2E), suggesting that the sp [2] and sp [3] structures in GO are intact after chemical crosslinking [8]. To confirm crystalline structures of fabricated sponges, a XRD analysis resulted in diffraction patterns of raw materials that showed a characteristic GO peak at 11.9° while Aln appeared as a large number of diffraction peaks (Fig. 2F). However, these peaks all disappeared after crosslinking, indicating that the crystalline structures of GO and Aln are changed and the fabricated sponges exhibit amorphous crystalline structures [39].

3.3. Effects of fabricated sponges on cell viability and proliferation

Live/Dead assay results showed that most BMSCs survived on the sponges, but the number of living cells (Fig. 3A, green) in Col-0.2%GO-Aln sponge was the lowest among four groups. In addition, SEM images of cell-sponge constructs with suitable cell density can clearly show the morphology of cells on the sponge, such as spreading area and pseudopod [40]. Fig. 3B exhibited the adhesive cells and secreted extracellular matrix on the sponges (pseudo-gold).

To investigate the effect of sponges on cell proliferation, we quantified BMSCs after treatment with extracts at 1, 3 and 7 days. Results of the CCK-8 assay showed that a significant reduction in rates of cell proliferation in Col-0.2%GO-Aln sponge compared to the other sponges (Fig. 3C).

3.4. Effects of fabricated sponges on osteogenic differentiation of BMSCs in vitro

The effect of sponges on osteogenic differentiation of BMSCs was evaluated by ALP and ARS staining. The ALP activity of BMSCs in Col-0.05%GO-Aln group was significantly increased compared to the other three groups (Fig. 4A and B). Analysis of images from the ARS staining revealed that the number of calcium nodules deposited by cells in Col-0.05%GO-Aln and Col-0.2%GO group was greater than that in Col-0.05%GO and Col-0.2%GO-Aln groups (Fig. 4A and C). Collectively, these results demonstrate that the Col-0.05%GO-Aln sponge exhibited a positive effect on *in vitro* osteoblastogenesis of BMSCs.

3.5. Effects of fabricated sponges on osteoclastogenesis of BMMs in vitro

BMMs isolated from rat bone marrow appeared small with a circular morphology. In addition, they proliferated in presence of M-CSF (Fig. 5A). When cultured with M-CSF and RANKL for 4 days, the BMMs were observed to induced formation of multinucleated and TRAP-positive osteoclasts (Fig. 5B). Based on this, the BMMs were cultured with extracts from fabricated sponges incorporated in M-CSF and RANKL for 4 days, followed by analysis of effects of fabricated sponges on osteoclastogenesis using TRAP staining and F-actin immunofluorescent staining. Images from the TRAP staining showed a diminishing number and area of TRAP-positive osteoclasts in the Col-0.05%GO-Aln and Col-0.2%GO-Aln sponges indicating suppression of osteoclast formation (Fig. 5C and D). The TRAP activity assay (Fig. 5E) indicated a consistent result with TRAP staining. The cell viability of BMMs following a 4-day

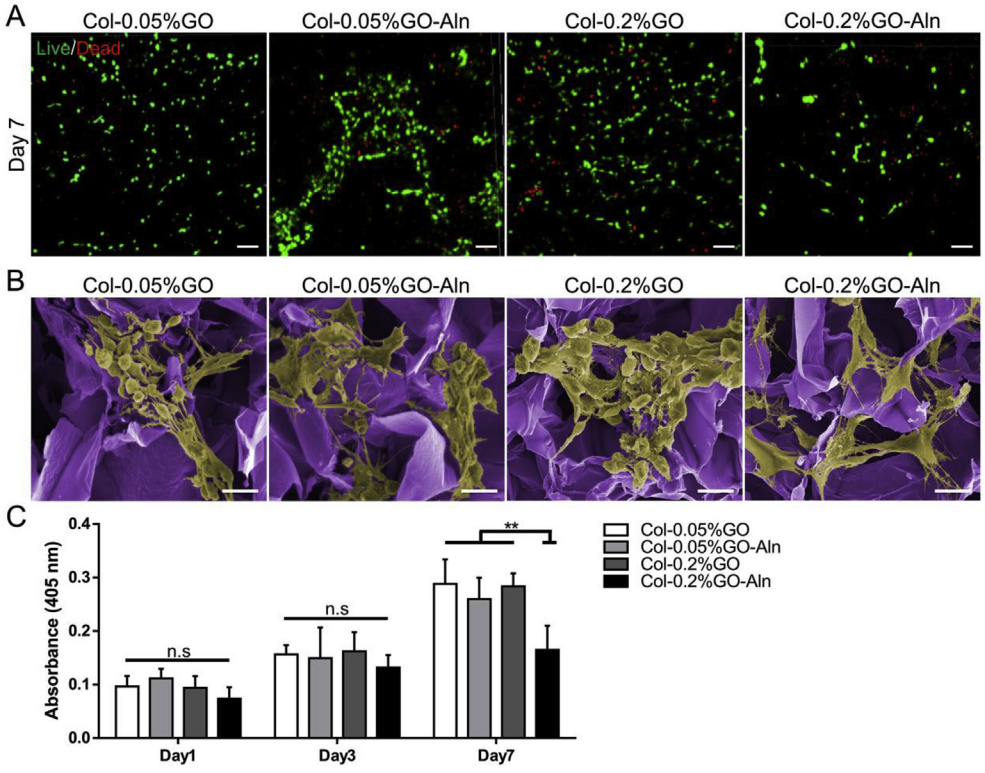

Fig. 3. Effects of Col-GO-Aln Sponges on Cell Viability and Proliferation. (A) Live/dead staining revealed that the amount of BMSCs survived on the Col-0.2%GO-Aln sponge was the lowest among four groups. (B) SEM images showed the morphology of the cells (pseudo-gold) on the sponges and the existence of secreted extracellular matrix. (C) CCK8 assays quantitatively indicated that the sponges did not compromise the proliferation of BMSCs, except for Col-0.2%GO-Aln sponges. (n = 5, n.s: no significance, *: P < 0.05, **: P < 0.01; scale bars in A: 100 μm, in B: 20 μm).

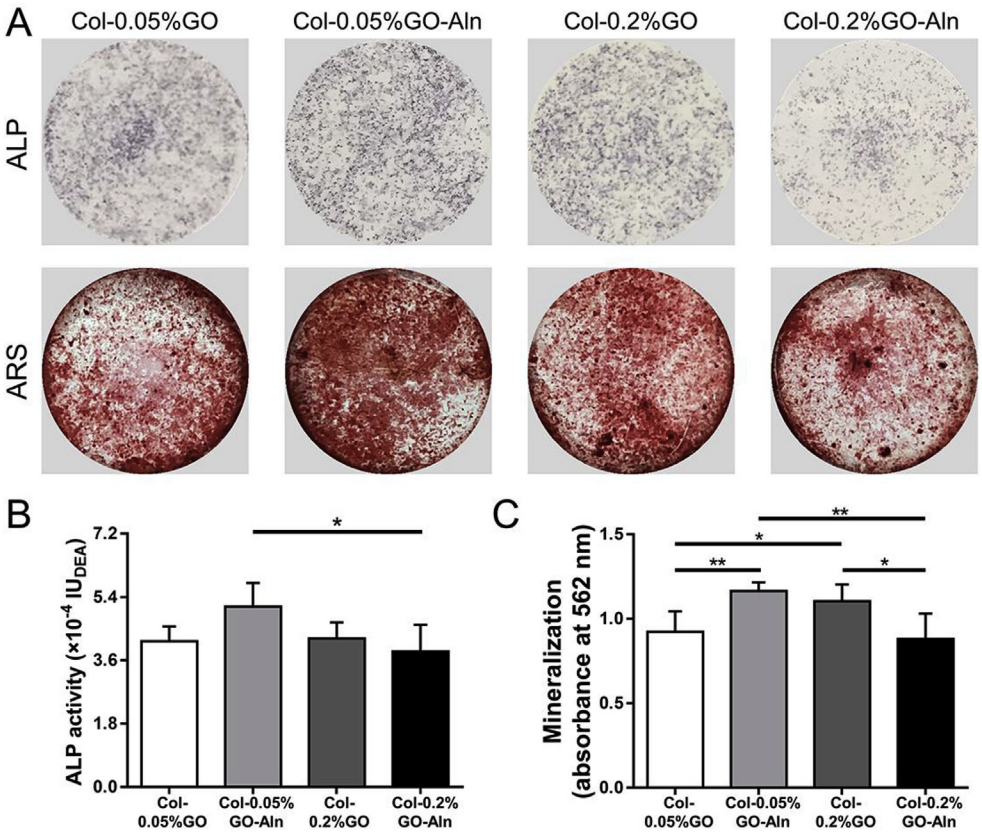

Fig. 4. Effects of Col-GO-Aln sponges on osteogenic differentiation of BMSCs *in vitro*. (A) As evidenced by ALP staining, Col-0.05%GO-Aln sponge promoted the ALP synthesis in BMSCs. (B) The ALP activity was also significantly increased in cells treated with Col-0.05%GO-Aln sponge. Moreover, ARS staining (A) and semi-quantitative analysis (C) showed that Col-0.05%GO-Aln and Col-0.2%GO sponges increased the calcium deposition of BMSCs. (n = 5, *: P < 0.05, **: P < 0.01.).

treatment with extracts containing M-CSF existed no differences among the four groups (Fig. 5F), indicating the suppression of osteoclast formation mentioned above was not associated with cytotoxicity of fabricated sponges to BMMs.

The formation of F-actins is considered a prerequisite for osteoclasts to resorb bone tissues [41]. Results from the phalloidin immunofluorescent staining showed that the F-actin rings were limited and localized in Col-0.05%GO-Aln and Col-0.2%GO-Aln groups. In addition, quantitative analysis of the number and size of F-actin rings (nucleus ≥ 3 is regarded as multinuclear osteoclast, while a nucleus ≥ 7 is considered mature osteoclast) further confirmed the inhibition on osteoclasts in Col-0.05%GO-Aln and Col-0.2%GO-Aln sponges (Fig. 5G and H). A comparison of the formation of F-actin ring in BMMs treated with extracts of Col, Col-0.05%GO and Col-0.2%GO sponges resulted in no differences indicating that GO has no marked influence on osteoclastogenesis of BMMs (Fig. S2).

3.6. Characterization of osteoporotic rat models

After ovariectomy three months, micro-CT images showed a reduced amount of trabecular bone in femur of OVX rats compared to the Sham group. Similarly, quantitative analysis showed that OVX rats had reduced bone mineral density and sparse trabecular bone tissues (Figs. S3A and B). The H&E staining of femur showed that the trabecular bone in metaphysis of OVX rat was limited (Fig. S3C).

After implantation, H&E staining of the liver, kidney and brain of experimental animals showed no inflammatory responses and tissue necrosis (Fig. S4), indicating the Col-GO-Aln sponges exist no noteworthy side effects to osteoporotic rat model.

3.7. Micro-CT and histological evaluation of the effect of fabricated sponges on bone regeneration

Coronal and sagittal 3D views showed that calvarial bone defects implanted with Col-0.05%GO-Aln sponges exhibited the best bone regeneration outcomes (Fig. 6A). The defects in rats of Col-0.05%GO-Aln group were bridged with newly formed bone, but in other groups regenerated limited bone tissue at 12 weeks post implantation. Quantitative analysis confirmed that the Col-0.05%GO-Aln sponge had more new bone volume (8.46 ± 2.44 mm^3) and higher BV/TV ratio (47.24 ± 12.00%) than in the other sponges (Fig. 6B).

To further visualize the newly-formed bone tissue in defect areas, we carried out H&E and Masson staining of skull samples. We found that defects in the Col-0.05%GO-Aln group exhibited many bone formation islands and achieved complete bridging repair, but those in other groups were replaced with fibrous tissues (Fig. 6C). In addition, we observed that GO remained in the bone defect area of all groups after 12 weeks and was significantly higher in Col-0.2%GO and Col-0.2%GO-Aln than in Col-0.05%GO and Col-0.05%GO-Aln groups. Furthermore, immunohistochemical staining analysis preformed to evaluate amount of osteoblast in regenerated bone tissue showed that the Col-0.05%GO-Aln group had higher expression levels of OCN, a marker of mature osteoblasts, than the other groups [42]. This indicates that Col-0.05%GO-Aln sponge effectively enhanced osteoblastogenesis in newly-formed bone tissue.

3.8. Micro-CT and histological evaluation of the effect of fabricated sponges on bone loss

To understand the effect of Col-GO-Aln sponges on bone loss during osteoporosis, we utilized micro-CT and histological measurements to analyze leftward femur of OVX rats after three months of implantation. According to 3D reconstructed images of the distal femoral metaphysis by micro-CT scan, coronal and lateral views showed numerous and denser trabecular bones reserved in rats of Col-0.05%GO-Aln and Col-0.2%GO-Aln groups, compared to those in Col-0.05%GO and Col-0.2%GO groups (Fig. 7A). In addition, quantification of trabecular bone parameters presented as BV/TV, BMD, Tb.N and Tb.Sp indicated the

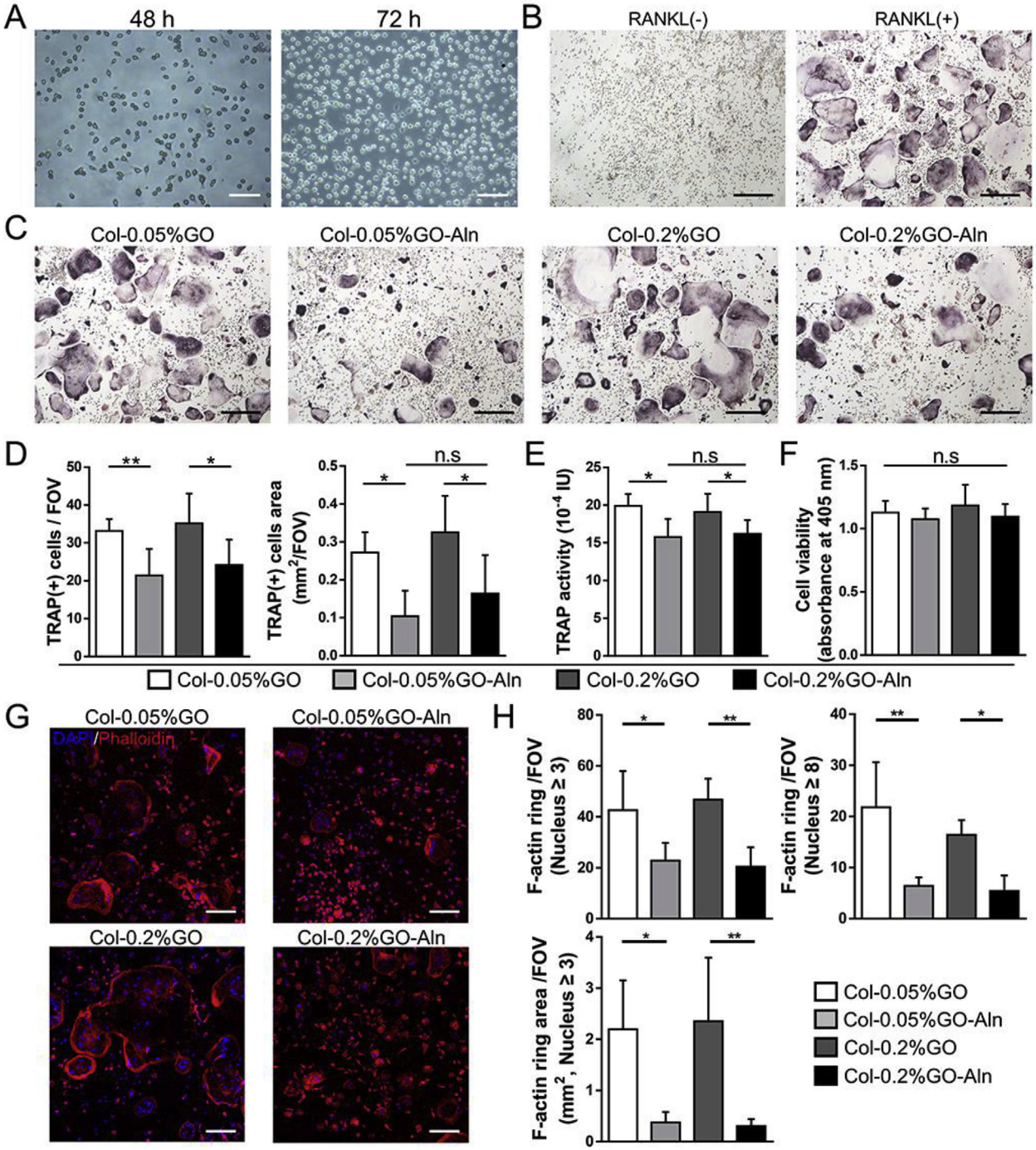

Fig. 5. Effects of Col-GO-Aln sponges on osteoclastogenesis of BMMs *in vitro*. (A) Rat BMMs were isolated and cultured with M-CSF for 72 h before osteoclastogenesis induction. (B) TRAP staining verified that RANKL treatment for 4 days induced the transformation of BMMs into TRAP-positive osteoclasts. The TRAP staining (C), quantitative analysis of number and area of TRAP-positive osteoclasts (D) and TRAP activity assays (E) revealed that Col-0.05%GO-Aln and Col-0.2%GO-Aln sponges inhibited the formation of osteoclasts and suppressed the expression of TRAP. Of note, the effect of the four sponges on the viability of BMMs (F) were comparable. Similarly, F-actin immunofluorescent staining of the osteoclasts (G) and the corresponding quantitative analysis (H) further revealed that the Col-0.05%GO-Aln and Col-0.2%GO-Aln sponges suppressed osteoclastogenesis. (n = 5, *: P < 0.05, **: P < 0.01, n.s: no significance; scale bars in A: 100 μm, in B and C: 500 μm, in G: 200μm.).

beneficial effects of Col-0.05%GO-Aln and Col-0.2%GO-Aln sponges in attenuating bone loss (Fig. 7B).

Images from histological analysis further showed that the trabecular bone structure reserved in femoral metaphysis of rats in Col-0.05%GO-Aln and Col-0.2%GO-Aln groups was more than that from the other two groups (Fig. 7C). Active osteoclasts evaluation, visualized following TRAP staining, showed that osteoclasts were limited in the metaphysis of OVX rats implanted with Col-0.05%GO-Aln and Col-0.2%GO-Aln sponges (Fig. 7D). Statistical analysis of the OC. S/BS and N. OC/BS indices indicated that bone resorption was significantly reduced in Col-0.05%GO-Aln and Col-0.2%GO-Aln groups (Fig. 7E). This suggests that *in vivo* implantation of Col-0.05%GO-Aln and Col-0.2%GO-Aln sponges can lead to inhibition of osteoclastogenesis and suppression of bone loss in osteoporosis.

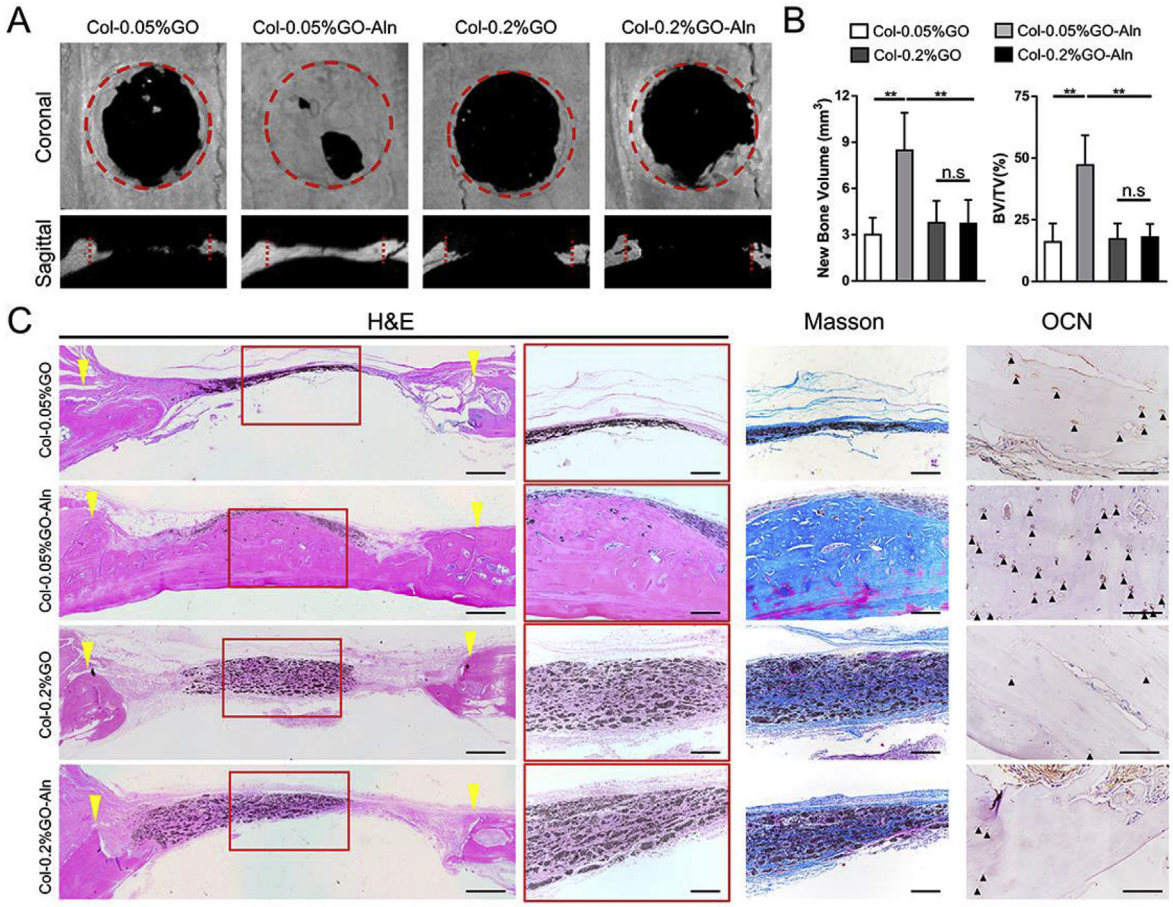

Fig. 6. The repair of Col-GO-Aln sponges on calvarial defect in OVX rats. (A) Three months after implantation, micro-CT images revealed that the Col-0.05%GO-Aln sponge repaired the calvarial defect of OVX rats but the other sponges were not yield significant repair. (B) Quantitative analysis indicated that the new bone volume in defect and bone volume/tissue volume (BV/TV) were higher in Col-0.05%GO-Aln group than in the other three groups. (C) H&E and Masson's staining showed that in Col-0.05%GO-Aln group, large quantities of hyperchromatic bone tissue were formed at the defect site. Moreover, a larger number of OCN-positive osteoblasts (black arrows) were present in the new bone of Col-0.05%GO-Aln group compared to other groups. (n = 6, **: $P < 0.01$, n.s: no significance; dotted red circle and yellow arrows: initial defect edge; scale bars in H&E staining: 500 μm and 200 μm, in Masson staining: 200 μm, in OCN staining: 100 μm).

Micro-CT images (A) and quantitative analysis (B) exhibited the higher BV/TV, bone mineral density (BMD), trabecula number (Tb.N) of the femurs and lower trabecula separation (Tb.Sp) in the groups containing Aln compared to the groups without Aln. (C) H&E and Masson staining showed more trabecula (yellow arrows) in metaphysis of rat in Col-0.05%GO-Aln and Col-0.2%GO-Aln groups. Moreover, TRAP staining (D) and quantitative analysis of indexes of bone resorption (E) showed that the sponges containing Aln apparently reduced the number of osteoclasts (red arrows) in the femoral metaphysis. (n = 6, **: $P < 0.01$, n.s: no significance; scale bars in H&E staining: 500 μm and 200 μm, in Masson staining: 200 μm, in TRAP staining: 100 μm; OC.S/BS: osteoclast surface/trabecular bone surface, N.OC/BS: number of osteoclast per trabecular bone surface).

4. Discussion

In this study, we fabricated Col-GO-Aln sponges using different proportions of GO, and compared their effects on osteogenic differentiation of BMSCs and osteoclastogenesis of BMMs *in vitro*. In addition, we analyzed the potentials of these sponges to repair osteoporotic bone defects as well as their ability to limit bone loss using *in vivo* assays. Our results showed that Col-0.05%GO-Aln sponge exhibited the biocompatible and bioactive performances required for bone regeneration in osteoporosis, and further attenuated systemic bone loss.

Based on experimental findings, we consider the variation in GO proportions has influenced the performance of Col-GO-Aln sponges in many aspects including structural characterization, drug releasing kinetics and biocompatibility. The findings indicated that an increase in GO in the fabricated Col-GO-Aln sponges resulted in significant structural changes evidenced by shapeless and disperse appearance of the sponge with 0.5% GO. It has been reported that different proportions of GO in hydrogels affect the degree of crosslinking between the amino group of polymers and the carboxyl groups in GO, further affecting the structural and mechanical properties of the sponges [8]. For example, the porosity of col-0.05% GO sponge and Col-0.2%GO sponge was similar but the water absorption rate was different, which could be attributed to the different degree of cross-linking. Our previous study also revealed that the mechanical properties of collagen sponges were positively related to the proportion of GO from 0 to 0.2% [24]. We speculated that a relatively high proportion of GO in the Col-GO-Aln sponge, such as 0.3 and 0.5%, would be insufficient in the degree of crosslinking because of the mismatched ratio in amino groups and carboxyl groups, and resulting in a loose and shapeless sponge.

We suggested that an increase in GO proportions may reduce the rate of Aln release by Col-GO-Aln sponge. The previous study has reported that special π–π bond and rich oxygen groups of GO were shown to facilitate an enhanced force between drugs and GO, thereby prolonging the duration of drug release [43]. In this study, we observed that the release rate was fast in the first 4 days and slowdown in the following period. The release process *in vitro* of Aln from the fabricated sponges seemed to be consistent with a first-order release. We considered that Aln rapidly released in early was physically entrapped in

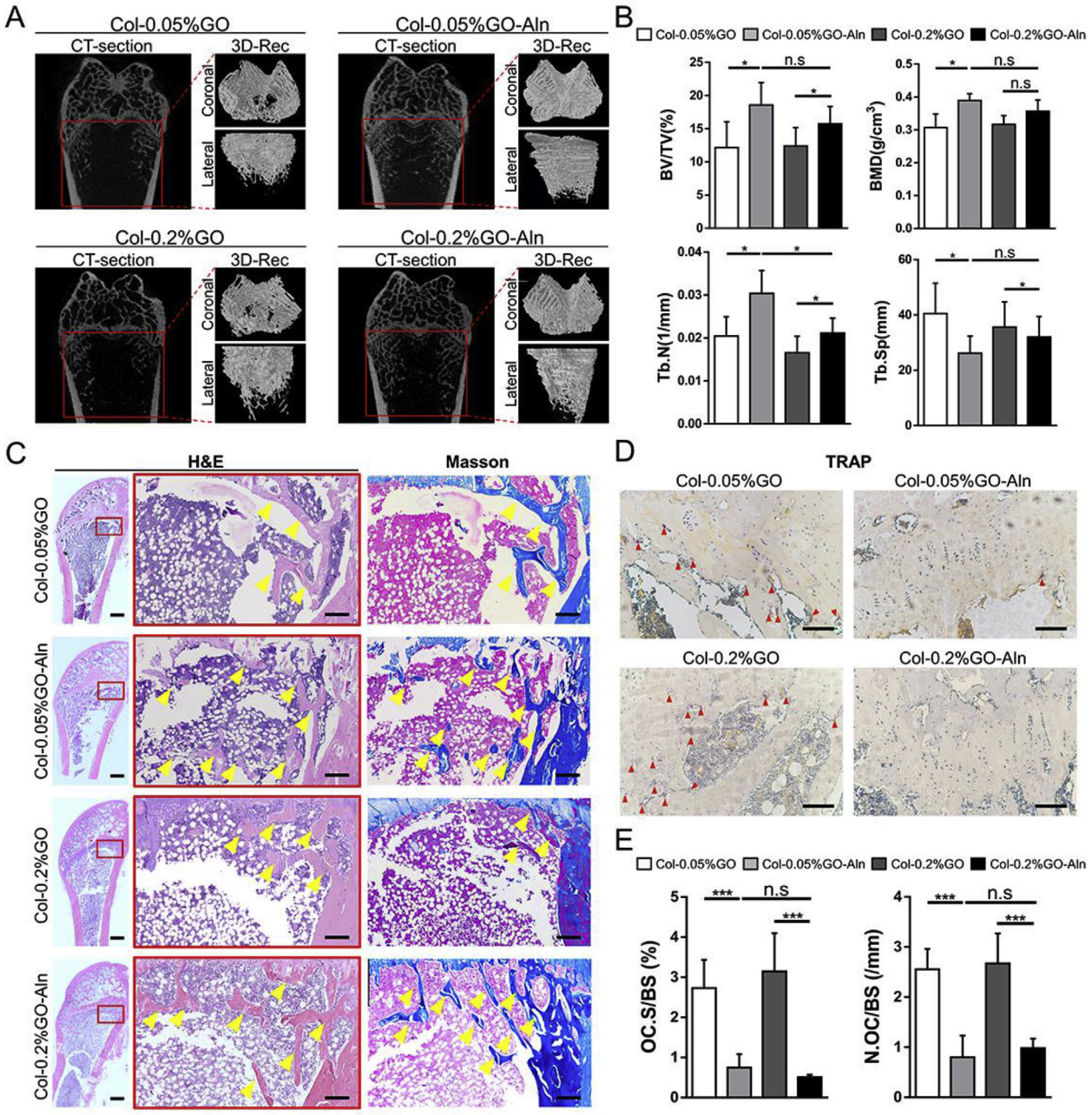

Fig. 7. Assessment of bone loss in OVX rats after implantation of Col-GO-Aln sponges.

sponges, and the subsequent released Aln had a tighter connection with sponges, resulting in a decrease in the release rate. The increase in GO concentration (0.2%) provided more oxygen groups and π bond to form the tighter linking in Col-GO-Aln sponge, which in turn exhibited a slower release rate. In addition, each Col-GO-Aln sponge was loaded with nearly 50 μg of Aln and released about 30 μg in one month. It can be speculated that the remaining Aln may link to GO with the help of EDC as previously reported, and this part of Aln will be released with the degradation of the sponge [30].

Biocompatibility of fabricated sponges are also influenced by the proportion of incorporated GO. Although GO is taken up and degraded by macrophages and finally excreted out of the body through kidneys, side effects have been described to occur when exaggerated quantities of the compound are applied *in vivo* [44]. For instance, Lu et al. implicated GO in gene damages in human embryonic kidney cell line (HEK293T) and zebrafish embryos [45]. Yang et al. found that GO exposure up-regulated mRNA levels of pro-inflammatory cytokines and increased the risk of neurotoxicity [46]. Considering such safety concerns of GO, it is essential to investigate appropriate concentrations to be incorporated into biomaterials. In this study, we evaluated the effects of Col-GO-Aln sponges on viability and proliferation of BMSCs. The results showed a marked decrease in ability of BMSCs to proliferate in Col-0.2%GO-Aln group. There could be three reasons for the restricted proliferation capacity: (1) cytotoxicity of GO, (2) BMSCs were undergoing differentiation into other cells and (3) cytotoxicity of Aln [8,44,47]. Notably, cells in Col-0.05%GO-Aln and Col-0.2%GO groups did not exhibit a significant decrease in proliferation compared to Col-0.05%GO groups. Based on this, we reasoned that a combination of Aln and 0.2% GO might generate a synergistic effect that exacerbates the cytotoxicity of Col-0.2%GO-Aln sponge. Biomaterials containing this superposed cytotoxicity are not conducive for proliferation and differentiation of cells within them, further losing the effect of improving osteoporotic bone metabolism.

Osteoporosis is a process characterized by insufficient

osteoblastogenesis of MSCs and overactive osteoclastogenesis [12]. Approaches aimed at restoring metabolic homeostasis in the bone have been proved beneficial interventions for repairing osteoporotic bone defects [48–50]. We found that GO promoted osteogenic differentiation of BMSCs, owing to presence of higher calcium nodules in Col-0.2%GO than Col-0.05%GO group. The effect of GO on osteoblastogenesis can attribute to its special structure which aid in accumulation of osteogenic factors such as OCN, OPN and BMP [8]. In addition, the oxygen groups on the surface of GO make deposition of minerals easier [51]. This study further found that the Col-0.05%GO-Aln sponge exhibited a higher osteogenic ability than Col-0.05%GO but the Col-0.2%GO-Aln sponge showed a lower osteogenic ability than Col-0.2%GO. Reports have shown that Aln stimulates osteogenic differentiation in MSCs by activating the ERK and JNK signaling pathways [52]. In this study, Aln enhanced osteogenic effect of the Col-0.05%GO-Aln sponge, but exacerbated cytotoxicity in Col-0.2%GO-Aln sponge resulting in impaired osteogenic differentiation of BMSCs in the Col-0.2%GO-Aln group.

Previous studies reported that Aln can inhibit osteoclast formation through suppression of ERK1/2 and Akt activations [53]. In this study, TRAP and F-actin staining as well as the corresponding quantitative analyses showed that Col-0.05%GO-Aln and Col-0.2%GO-Aln sponges had restricted the number and area of osteoclasts compared to the Aln-free ones. A recent study demonstrated that GO, as a drug carrier, can be phagocytized into osteoclasts, but it was not shown whether this compound could inhibit osteoclast maturation [54]. In our study, a comparison among Aln-free groups of sponges with different proportion of GO showed similar results indicating that osteoclastogenesis was not influenced. It is possible that GO was taken up then degraded by osteoclasts resulting in no notable influence on activity of osteoclasts.

We also noted that Col-0.05%GO-Aln sponge not only showed a regulatory effect on osteoblastogenesis and osteoclastogenesis *in vitro* but also performed significantly well in repair of osteoporotic bone defects *in vivo*. In the process of bone regeneration, osteoblasts play a key role in secreting organic bone matrix and cytokines like VEGF [55,56]. They are also involved in harnessing mineral deposits to construct new bone tissue [57]. We noted a higher number of OCN-positive cells in the newborn bone tissue of Col-0.05%GO-Aln group relative to that in other groups. When implanted into the bone defect, the sponge attracts surrounding MSCs initiating migration into the material and subsequently inducing osteogenic differentiation of cells. Col-0.05%GO-Aln sponge is beneficial to osteoblastogenesis of the impaired cells in osteoporosis and this ensures adequate repair of the osteoporotic bone defect. In addition, a relatively large amount of GO remaining in the tissues may be the other reason for the limited regeneration of bone tissue in the Col-0.2%GO and Col-0.2%GO-Aln group due to the increased degree of inflammation and toxicity of this compound.

Bone resorption hyperactivity in osteoporosis occurs in the whole-body skeleton [58]. A meaningful finding of our research is the attenuation of the femur metaphysis bone loss in OVX rats by Col-0.05%GO-Aln and Col-0.2%GO-Aln sponges. Commonly, the systemic effects of local drug delivery could have been as a result of direct diffusion of the released drug into surrounding tissues and distal transportation through the circulation [59]. In this study, Aln was released from Col-GO-Aln sponges to tissue fluid after implantation and then entered into blood through the reabsorption of capillaries. This *in vivo* process was affected by factors such as the volume of tissue fluid immersed in the sponge and the time for the drug to stay in the tissue around the calvarial defect. Therefore, compared with oral administration, it is difficult to determine the period when the locally delivered Aln enters the circulation, but the drug will continue to be released from Col-GO-Aln sponges and resist bone loss.

5. Conclusion

In summary, the Aln loaded Col-GO sponge has exhibited active anti-osteoclastogenesis and osteogenesis ability *in vitro* and in osteoporotic rats. By such a drug-loading system, sustained release of Aln has been successfully achieved for a month. At the same time, our study suggests the potential of GO related hydrogel in the treatment of osteoporotic bone defects.

CRediT authorship contribution statement

Yuyang Zeng: Conceptualization, Methodology, Data curation, Writing - original draft. **Muran Zhou:** Conceptualization, Methodology, Writing - original draft. **Lifeng Chen:** Data curation. **Huimin Fang:** Data curation. **Shaokai Liu:** Investigation. **Chuchao Zhou:** Software, Visualization. **Jiaming Sun:** Supervision, Writing - review & editing. **Zhenxing Wang:** Writing - review & editing, Project administration.

Declaration of competing interest

The authors declared that they have no conflicts of interest to this work.

Acknowledgements

This work was supported by the National Key R&D Program of China (2019YFA0110500) and the National Natural Science Foundation of China (81701922, 81873941).

Appendix A. Supplementary data

Supplementary data to this article can be found online at https://doi.org/10.1016/j.bioactmat.2020.06.010.

References

[1] S.R. Shin, Y.C. Li, H.L. Jang, P. Khoshakhlagh, M. Akbari, A. Nasajpour, Y.S. Zhang, A. Tamayol, A. Khademhosseini, Graphene-based materials for tissue engineering, Adv. Drug Deliv. Rev. 105 (2016) 255–274.
[2] H. Gao, H. Duan, 2D and 3D graphene materials: preparation and bioelectrochemical applications, Biosens. Bioelectron. 65 (2015) 404–419.
[3] Q. Mei, B. Liu, G. Han, R. Liu, M.Y. Han, Z. Zhang, Graphene oxide: from tunable structures to diverse luminescence behaviors, Advanced science 6 (14) (2019) 1900855.
[4] L. Ouyang, Y. Deng, L. Yang, X.Y. Shi, T.S. Dong, Y.Y. Tai, W.Z. Yang, Z.G. Chen, Graphene-oxide-decorated microporous polyetheretherketone with superior antibacterial capability and in vitro osteogenesis for orthopedic implant, Macromol. Biosci. 18 (2018) 1800036.
[5] Y. Deng, X.Y. Gao, X.L. Shi, S.Y. Lu, W.Z. Yang, C.Y. Duan, Z.G. Chen, Graphene oxide and adiponectin-functionalized sulfonated poly(etheretherketone) with effective osteogenicity and remotely repeatable photodisinfection, Chem. Mater. 32 (2020) 2180–2193.
[6] H.S. Song, O.S. Kwon, J.H. Kim, J. Conde, N. Artzi, 3D hydrogel scaffold doped with 2D graphene materials for biosensors and bioelectronics, Biosens. Bioelectron. 89 (2017) 187–200.
[7] R. Patil, V. Kansara, D. Ray, V.K. Aswal, P.K. Jha, P. Bahadur, S. Tiwari, Slow degrading hyaluronic acid hydrogel reinforced with cationized graphene nanosheets, Int. J. Biol. Macromol. 141 (2019) 232–239.
[8] J. Ruan, X. Wang, Z. Yu, Z. Wang, Q. Xie, D. Zhang, Y. Huang, H. Zhou, X. Bi, C. Xiao, P. Gu, X. Fan, Enhanced physiochemical and mechanical performance of chitosan-grafted graphene oxide for superior osteoinductivity, Adv. Funct. Mater. 26 (2016) 1085–1097.
[9] Y. Chen, Z. Zheng, R. Zhou, H. Zhang, C. Chen, Z. Xiong, K. Liu, X. Wang, Developing a strontium-releasing graphene oxide-/collagen-based organic-in-organic nanobiocomposite for large bone defect regeneration via MAPK signaling pathway, ACS Appl. Mater. Interfaces 11 (2019) 15986–15997.
[10] J. Venkatesan, R. Pallela, S.K. Kim, Applications of carbon nanomaterials in bone tissue engineering, J. Biomed. Nanotechnol. 10 (2014) 3105–3123.
[11] G. Choe, S. Oh, J.M. Seok, S.A. Park, J.Y. Lee, Graphene oxide/alginate composites as novel bioinks for three-dimensional mesenchymal stem cell printing and bone regeneration applications, Nanoscale 11 (2019) 23275.
[12] C.X. Zheng, B.D. Sui, X.Y. Qiu, C.H. Hu, Y. Jin, Mitochondrial regulation of stem cells in bone homeostasis, Trends Mol. Med. 26 (2020) 89–104.
[13] J. Tan, L. Zhou, Y. Zhou, P. Xue, G. Wu, G. Dong, H. Guo, Q. Wang, The influence of diabetes mellitus on proliferation and osteoblastic differentiation of MSCs, Curr. Stem Cell Res. Ther. 12 (2017) 388–400.
[14] B.D. Sui, C.H. Hu, C.X. Zheng, Y. Jin, Microenvironmental views on mesenchymal stem cell differentiation in aging, J. Dent. Res. 95 (2016) 1333–1340.

[15] T. Hiraga, Hypoxic microenvironment and metastatic bone disease, Int. J. Mol. Sci. 19 (2018) 3523.
[16] C.-X. Zheng, B.-D. Sui, X.-Y. Qiu, C.-H. Hu, Y. Jin, Mitochondrial regulation of stem cells in bone homeostasis, Trends Mol. Med. 26 (2020) 89–104.
[17] C. Schlundt, C.H. Bucher, S. Tsitsilonis, H. Schell, G.N. Duda, K. Schmidt-Bleek, Clinical and research Approaches to treat non-union fracture, Curr. Osteoporos. Rep. 16 (2018) 155–168.
[18] Z. Wang, D. Wu, J. Zou, Q. Zhou, W. Liu, W. Zhang, G. Zhou, X. Wang, G. Pei, Y. Cao, Development of demineralized bone matrix based implantable and biomimetic microcarrier for stem cell expansion and single-step tissue-engineered bone graft construction, J. Mater. Chem. B 5 (2017) 62–73.
[19] B. Roche, A. Vanden-Bossche, L. Malaval, M. Normand, M. Jannot, R. Chaux, L. Vico, M.H. Lafage-Proust, Parathyroid hormone 1-84 targets bone vascular structure and perfusion in mice: impacts of its administration regimen and of ovariectomy, J. Bone Miner. Res. 29 (2014) 1608–1618.
[20] A. Spangenberg, N. Maghsoodi, D. Dulnoan, A.E. Moore, S. Edwards, M.L. Frost, G. Hampson, Bone mineral density and body composition are associated with circulating angiogenic factors in post-menopausal women, Calcif. Tissue Int. 99 (2016) 608–615.
[21] L. Cao, G. Liu, Y. Gan, Q. Fan, F. Yang, X. Zhang, T. Tang, K. Dai, The use of autologous enriched bone marrow MSCs to enhance osteoporotic bone defect repair in long-term estrogen deficient goats, Biomaterials 20 (2012) 5076–5084.
[22] X. Yu, X. Tang, S.V. Gohil, C.T. Laurencin, Biomaterials for bone regenerative engineering, Advanced healthcare materials 4 (2015) 1268–1285.
[23] X. Cui, Y. Zhang, J. Wang, C. Huang, Y. Wang, H. Yang, W. Liu, T. Wang, D. Wang, G. Wang, C. Ruan, D. Chen, W. Lu, W. Huang, M. Rahaman, H. Pan, Strontium modulates osteogenic activity of bone cement composed of bioactive borosilicate glass particles by activating Wnt/β-catenin signaling pathway, Bioactive materials 5 (2020) 334–347.
[24] S. Liu, S. Mou, C. Zhou, L. Guo, A. Zhong, J. Yang, Q. Yuan, J. Wang, J. Sun, Z. Wang, Off-the-Shelf biomimetic graphene oxide-collagen hybrid scaffolds wrapped with osteoinductive extracellular matrix for the repair of cranial defects in rats, ACS Appl. Mater. Interfaces 10 (2018) 42948–42958.
[25] T. Wu, J. Sun, L. Tan, Q. Yan, L. Li, L. Chen, X. Liu, S. Bin, Enhanced osteogenesis and therapy of osteoporosis using simvastatin loaded hybrid system, Bioactive materials 5 (2020) 348–357.
[26] M. Sakata, H. Tonomura, T. Itsuji, H. Ishibashi, R. Takatori, Y. Mikami, M. Nagae, K.I. Matsuda, Y. Tabata, M. Tanaka, T. Kubo, Bone regeneration of osteoporotic vertebral body defects using platelet-rich plasma and gelatin beta-tricalcium phosphate sponges, Tissue Eng. 24 (2018) 1001–1010.
[27] D. Zheng, K.G. Neoh, E.T. Kang, Immobilization of alendronate on titanium via its different functional groups and the subsequent effects on cell functions, J. Colloid Interface Sci. 487 (2017) 1–11.
[28] A. Tang, Y. Qian, S. Liu, W. Wang, B. Xu, A. Qin, G. Liang, Self-assembling bisphosphonates into nanofibers to enhance their inhibitory capacity on bone resorption, Nanoscale 8 (2016) 10570–10575.
[29] H. Quan, Y. He, J. Sun, W. Yang, W. Luo, C. Dou, F. Kang, C. Zhao, J. He, X. Yang, S. Dong, H. Jiang, Chemical self-assembly of multifunctional hydroxyapatite with a coral-like nanostructure for osteoporotic bone reconstruction, ACS Appl. Mater. Interfaces 10 (2018) 25547–25560.
[30] T.T. Pham, H.T. Nguyen, C.D. Phung, S. Pathak, S. Regmi, D.H. Ha, J.O. Kim, C.S. Yong, S.K. Kim, J.E. Choi, S. Yook, J.B. Park, J.H. Jeong, Targeted delivery of doxorubicin for the treatment of bone metastasis from breast cancer using alendronate-functionalized graphene oxide nanosheets, J. Ind. Eng. Chem. 76 (2019) 310–317.
[31] J. Li, C. Zhou, C. Luo, B. Qian, S. Liu, Y. Zeng, J. Hou, B. Deng, Y. Sun, J. Yang, Q. Yuan, A. Zhong, J. Wang, J. Sun, Z. Wang, N-acetyl cysteine-loaded graphene oxide-collagen hybrid membrane for scarless wound healing, Theranostics 9 (2019) 5839–5853.
[32] M.I. Walash, M.E. Metwally, M. Eid, R.N. El-Shaheny, Validated spectrophotometric methods for determination of Alendronate sodium in tablets through nucleophilic aromatic substitution reactions, Chem. Cent. J. 6 (2012) 25.
[33] X. Wang, D. Zeng, W. Weng, Q. Huang, X. Zhang, J. Wen, J. Wu, X. Jiang, Alendronate delivery on amino modified mesoporous bioactive glass scaffolds to enhance bone regeneration in osteoporosis rats, Artificial cells, nanomedicine, and biotechnology 46 (2018) 171–181.
[34] C.H. Zhou, Z.L. Shi, J.H. Meng, B. Hu, C.C. Zhao, Y.T. Yang, W. Yu, Z.X. Chen, B.C. Heng, V.A. Parkman, S. Jiang, H.X. Zhu, H.B. Wu, W.L. Shen, S.G. Yan, Sophocarpine attenuates wear particle-induced implant loosening by inhibiting osteoclastogenesis and bone resorption via suppression of the NF-kappaB signalling pathway in a rat model, Br. J. Pharmacol. 175 (2018) 859–876.
[35] Q. Tang, Z. Hu, H. Jin, G. Zheng, X. Yu, G. Wu, H. Liu, Z. Zhu, H. Xu, C. Zhang, L. Shen, Microporous polysaccharide multilayer coated BCP composite scaffolds with immobilised calcitriol promote osteoporotic bone regeneration both in vitro and in vivo, Theranostics 9 (2019) 1125–1143.
[36] K. Chen, Z.T. Lv, P. Cheng, W.T. Zhu, S. Liang, Q. Yang, V.A. Parkman, C.H. Zhou, X.Z. Jing, H. Liu, Y.T. Wang, H. Lin, H. Liao, A.M. Chen, Boldine ameliorates estrogen deficiency-induced bone loss via inhibiting bone resorption, Front. Pharmacol. 9 (2018) 1046.
[37] R. Deepachitra, V. Ramnath, T.P. Sastry, Graphene oxide incorporated collagen–fibrin biofilm as a wound dressing material, RSC Adv. 4 (2014) 62717–62727.
[38] S.E. Kim, Y.P. Yun, D.W. Lee, E.Y. Kang, W.J. Jeong, B. Lee, M.S. Jeong, H.J. Kim, K. Park, H.R. Song, Alendronate-eluting biphasic calcium phosphate (BCP) scaffolds stimulate osteogenic differentiation, BioMed Res. Int. (2015) 320713.
[39] G.M. Mekhail, A.O. Kamel, G.A. Awad, N.D. Mortada, R.L. Rodrigo, P.A. Spagnuolo, S.D. Wettig, Synthesis and evaluation of alendronate-modified gelatin biopolymer as a novel osteotropic nanocarrier for gene therapy, Nanomedicine 11 (2016) 2251–2273.
[40] T.S. Dong, C.Y. Duan, S. Wang, X.Y. Gao, Q.Z. Yang, W.Z. Yang, Y. Deng, Multifunctional surface with enhanced angiogenesis for improving long-term osteogenic fixation of poly(ether ether ketone) implants, ACS Appl. Mater. Interfaces 12 (2020) 14971–14982.
[41] M. Li, X. Chen, J. Yan, L. Zhou, Y. Wang, F. He, J. Lin, C. Zhu, G. Pan, J. Yu, M. Pei, H. Yang, T. Liu, Inhibition of osteoclastogenesis by stem cell-derived extracellular matrix through modulation of intracellular reactive oxygen species, Acta Biomater. 71 (2018) 118–131.
[42] J. Li, C. Liu, Y. Li, Q. Zheng, Y. Xu, B. Liu, W. Sun, Y. Li, S. Ji, M. Liu, J. Zhang, D. Zhao, R. Du, Z. Liu, G. Zhong, C. Sun, Y. Wang, J. Song, S. Zhang, J. Qin, S. Ling, X. Wang, Y. Li, TMCO1-mediated Ca(2+) leak underlies osteoblast functions via CaMKII signaling, Nat. Commun. 10 (2019) 1589.
[43] J. Liu, J. Dong, T. Zhang, Q. Peng, Graphene-based nanomaterials and their potentials in advanced drug delivery and cancer therapy, J. Contr. Release 286 (2018) 64–73.
[44] F.M. Tonelli, V.A. Goulart, K.N. Gomes, M.S. Ladeira, A.K. Santos, E. Lorenon, L.O. Ladeira, R.R. Resende, Graphene-based nanomaterials: biological and medical applications and toxicity, Nanomedicine 10 (2015) 2423–2450.
[45] C.J. Lu, X.F. Jiang, M. Junaid, Y.B. Ma, P.P. Jia, H.B. Wang, D.S. Pei, Graphene oxide nanosheets induce DNA damage and activate the base excision repair (BER) signaling pathway both in vitro and in vivo, Chemosphere 184 (2017) 795–805.
[46] X. Yang, Q. Yang, G. Zheng, S. Han, F. Zhao, Q. Hu, Z. Fu, Developmental neurotoxicity and immunotoxicity induced by graphene oxide in zebrafish embryos, Environ. Toxicol. 34 (2019) 415–423.
[47] N.O. Hodgins, W.T. Al-Jamal, J.T.-W. Wang, A.C. Parente-Pereira, M. Liu, J. Maher, K.T. Al-Jamal, In vitro potency, in vitro and in vivo efficacy of liposomal alendronate in combination with γδ T cell immunotherapy in mice, J. Contr. Release 10 (2016) 229–241.
[48] V. Nicolin, N. De Tommasi, S.L. Nori, F. Costantinides, F. Berton, R. Di Lenarda, Modulatory effects of plant polyphenols on bone remodeling: a prospective view from the bench to bedside, Front. Endocrinol. 10 (2019) 494.
[49] S. Maria, R.M. Samsonraj, F. Munmun, J. Glas, M. Silvestros, M.P. Kotlarczyk, R. Rylands, A. Dudakovic, A.J. van Wijnen, L.T. Enderby, H. Lassila, B. Dodda, V.L. Davis, J. Balk, M. Burow, B.A. Bunnell, P.A. Witt-Enderby, Biological effects of melatonin on osteoblast/osteoclast cocultures, bone, and quality of life: implications of a role for MT2 melatonin receptors, MEK1/2, and MEK5 in melatonin-mediated osteoblastogenesis, J. Pineal Res. 64 (2018).
[50] B. Lecka-Czernik, C.J. Rosen, Energy excess, glucose utilization, and skeletal remodeling: new insights, J. Bone Miner. Res. 30 (2015) 1356–1361.
[51] C. Zhou, S. Liu, J. Li, K. Guo, Q. Yuan, A. Zhong, J. Yang, J. Wang, J. Sun, Z. Wang, Collagen functionalized with graphene oxide enhanced biomimetic mineralization and in situ bone defect repair, ACS Appl. Mater. Interfaces 10 (2018) 44080–44091.
[52] P. Jiang, Z. Mao, C. Gao, Combinational effect of matrix elasticity and alendronate density on differentiation of rat mesenchymal stem cells, Acta Biomater. 19 (2015) 76–84.
[53] M. Tsubaki, M. Komai, T. Itoh, M. Imano, K. Sakamoto, H. Shimaoka, T. Takeda, N. Ogawa, K. Mashimo, D. Fujiwara, Nitrogen-containing bisphosphonates inhibit RANKL- and M-CSF-induced osteoclast formation through the inhibition of ERK1/2 and Akt activation, J. Biomed. Sci. 21 (2014) 10.
[54] C. Dou, N. Ding, F. Luo, T. Hou, Z. Cao, Y. Bai, C. Liu, J. Xu, S. Dong, Graphene-based MicroRNA transfection blocks preosteoclast fusion to increase bone formation and vascularization, Advanced science 5 (2018) 1700578.
[55] H. Jaha, D. Husein, Y. Ohyama, D. Xu, S. Suzuki, G.T. Huang, Y. Mochida, N-terminal Dentin Sialoprotein fragment induces type I collagen production and upregulates dentinogenesis marker expression in osteoblasts, Biochemistry and biophysics reports 6 (2016) 190–196.
[56] K. Hu, B.R. Olsen, Osteoblast-derived VEGF regulates osteoblast differentiation and bone formation during bone repair, J. Clin. Invest. 126 (2016) 509–526.
[57] T. Hasegawa, Ultrastructure and biological function of matrix vesicles in bone mineralization, Histochem. Cell Biol. 149 (2018) 289–304.
[58] B.H. Arjmandi, S.A. Johnson, S. Pourafshar, N. Navaei, K.S. George, S. Hooshmand, S.C. Chai, N.S. Akhavan, Bone-protective effects of dried plum in postmenopausal women: efficacy and possible mechanisms, Nutrients 9 (2017) 5.
[59] C.X. Zhou, L. Li, Y.G. Ma, B.N. Li, G. Li, Z. Zhou, F. Shi, J. Weng, C. Zhang, F. Wang, X. Cui, L. Wang, H. Wang, A bioactive implant in situ and long-term releases combined drugs for treatment of osteoarticular tuberculosis, Biomaterials 176 (2018) 50–59.